

We are IntechOpen, the world's leading publisher of Open Access books Built by scientists, for scientists

4,800

Open access books available

122,000

International authors and editors

135M

Downloads

Our authors are among the

154

Countries delivered to

TOP 1%

most cited scientists

12.2%

Contributors from top 500 universities



WEB OF SCIENCE™

Selection of our books indexed in the Book Citation Index
in Web of Science™ Core Collection (BKCI)

Interested in publishing with us?
Contact book.department@intechopen.com

Numbers displayed above are based on latest data collected.
For more information visit www.intechopen.com



Optimization problems for controlled mechanical systems: Bridging the gap between theory and application

M. Chyba^a, T. Haberkorn^b, R.N. Smith^c

^a *University of Hawaii, Honolulu, HI 96822 USA
Mathematics, College of Natural Sciences*

^b *Université d'Orléans, 45067 Orléans Cedex 2, France
Laboratoire MAPMO*

^c *University of Southern California, Los Angeles, CA 90089, USA
Robotic Embedded Systems Laboratory, Department of Computer Science*

1. Introduction

Mechanical control systems have become a part of our everyday life. Systems such as automobiles, robot manipulators, mobile robots, satellites, buildings with active vibration controllers and air conditioning systems, make life easier and safer, as well as help us explore the world we live in and exploit its available resources. In this chapter, we examine a specific example of a mechanical control system; the Autonomous Underwater Vehicle (AUV). Our contribution to the advancement of AUV research is in the area of guidance and control. We present innovative techniques to design and implement control strategies that consider the optimization of time and/or energy consumption.

Recent advances in robotics, control theory, portable energy sources and automation increase our ability to create more intelligent robots, and allows us to conduct more explorations by use of autonomous vehicles. This facilitates access to higher risk areas, longer time underwater, and more efficient exploration as compared to human occupied vehicles. The use of underwater vehicles is expanding in every area of ocean science. Such vehicles are used by oceanographers, archaeologists, geologists, ocean engineers, and many others. These vehicles are designed to be agile, versatile and robust, and thus, their usage has gone from novelty to necessity for any ocean expedition.

Formally, AUVs are characterized by a Lagrangian of the form kinetic energy minus potential energy. This is commonly referred to as the class of *simple* mechanical control systems, see (Lewis & Murray, 1997) and (Bullo & Lewis, 2004). Theoretically, an AUV is represented by a complex, non-linear, dynamic system of equations to model and control. Practically speaking, providing solutions to the motion planning problem, which considers the optimization of some cost function, will result in a more robust control scheme for the vehicle, and therefore increase its autonomy. Thus, an AUV poses an interesting research problem from both theoretical and practical viewpoints, and it is an excellent platform to generate advances in both areas simultaneously.

An interesting practical problem in the study of autonomous vehicles in general, is energy consumption. Since an AUV must carry its own power source throughout the entire duration of a mission, it is critical to consider the energy demands that certain control strategies or planned trajectories require. Hence, the theory behind a solution to the motion planning problem for AUVs must consider energy consumption to ensure that the solution is practically implementable. For example, in (Chyba et al., 2009a) the authors design control strategies that reduce the number of times the actuators are required to change direction. Such a strategy keeps the actuators operating in a steady-state, which reduces error in thrust application. Implementation results of these strategies onto a test-bed vehicle are presented, and match well with theoretical predictions. In addition, energy consumption for the presented strategies was kept near the computed minimum value.

Another practical concern for AUV implementation is under-actuation. Some vehicles are designed to operate in an under-actuated condition, while others fully-actuated vessels need to be prepared to deal with actuator failure(s) resulting from any number of mechanical issues. In an effort to conserve energy, it may be beneficial to operate an AUV in an under-actuated, but fully-controllable condition. Additionally, early consideration of under-actuated path planning results may assist in vehicle design to implement effective redundancy onto a vehicle. Such consideration at the design stage could also aid in the construction of a fully-controllable but under-actuated vehicle for more cost-effective applications. One approach to control strategy design for under-actuated vehicles is by use of kinematic reductions as done in (Smith, 2008) and (Smith et al., 2009a). Here, the authors designed control strategies for under-actuated AUVs and present the results of their implementation onto a test-bed vehicle. In these papers, the equations of motion for an AUV are derived in the framework of differential geometry. There are many advantages to describing a controlled mechanical system in this way (c.f., (Bullo & Lewis, 2004) and (Lewis, 2007)), thus it is the point of view that we adopt in the present chapter.

Based upon previous results presented in (Chyba et al., 2009a), (Smith, 2008) and (Smith et al., 2009a), we propose a control strategy design method that accounts for the two essential features necessary in the guidance and control of AUVs; namely minimizing energy consumption and incorporating under-actuation. The reader should keep in mind throughout this article, that bridging the gap between theory and application is our main goal. Hence, we are motivated to design control strategies that can be implemented onto a real vehicle, and not ones that can only be implemented in numerical simulations. For our specific AUV application, we need to design control strategies that are piecewise constant with respect to time, and that only require a small number of direction changes of the actuators. In this chapter, we neglect external uncertainties and disturbances, such as currents, as our experiments are conducted in the controlled environment of a swimming pool. Research is ongoing to merge the presented control strategies with existing adaptive control systems to account for external disturbances.

We remark that guidance and control of AUVs is not the only practical application dealing with cost optimization that requires the type of control structure we consider. In particular, research has shown that an ideal radiation delivery strategy for cancer treatment is to administer a period of intense treatment followed by period of rest. Continuous

drug administration is possible, but at this time requires long hospital stays, and is thus not practical. Research is ongoing to develop methods and materials for specialized drug delivery ((Ledzewicz & Schättler, 2009)). Another example of a system utilizing a piecewise constant control structure while minimizing energy consumption is a home heating and cooling system. It is impractical and inefficient for the system to continuously adjust the input air temperature to a home. This would require the system to remain powered on all the time. Instead, as has been established in many other optimal control problems, the optimal strategy has a *bang-bang* structure. This bang-bang structure is easy to implement in practice, however, optimal solutions may contain chattering, a large number of discontinuities (i.e., instantaneous changes in the control), which cannot be implemented on a physical system. To remedy this issue, we present the STP algorithm. This control strategy design algorithm provides an implementable solution to the optimization problem, while also keeping the optimization criteria close to optimal.

2. Modeling

In this chapter, we identify a simple control mechanical system with a second-order forced affine connection control system (FACCS) on a differentiable, configuration manifold, $Q = \mathbb{R}^3 \times \text{SO}(3) \cong \text{SE}(3)$. Our motivation is to exploit inherent geometric properties and symmetries of the mechanical system to provide solutions to the motion planning problem.

2.1 Mechanical Control Systems

An FACCS is a 5-tuple $(Q, \nabla, F, \mathcal{Y}, U)$, where Q is the configuration manifold for the system, ∇ is an affine connection defined on Q , F represents the external forces, \mathcal{Y} is a set of vector fields defined on Q and $U \subset \mathbb{R}^m$. We refer to the set \mathcal{Y} as the set of input control vector fields. If we assume \mathcal{Y} to be given by $\sum_{i=1}^m \sigma_i F_i$, the equations of motion take the form:

$$\nabla_{\gamma'} \gamma' = G^\#(F(\gamma'(t))) + \sum_{i=1}^m G^\# F_i(\gamma(t)) \sigma_i(t), \quad (1)$$

where $G^\#$ is the inverse of the kinematic energy metric G and ∇ is the Levi-Civita connection associated to G . The control $\sigma(\cdot)$ is a measurable bounded function that takes its values in U .

There is a vast amount of literature devoted to the study of mechanical control systems, the references listed here are only those that are directly related to our work.

2.1.1 Underwater Vehicles

The control strategies presented in the following sections were designed with the intention to implement them onto a test-bed AUV. Here, we do not present the experimental results from these implementations, however we refer the interested reader to (Smith, 2008) for results of the implementation of the kinematic control strategies given in the simulation section onto a test-bed AUV.

A very detailed description of the equations of motion for a submerged rigid body can be found in (Smith et al., 2009a). In this chapter we just briefly recall these results to introduce the model. The equations of motion for a general simple mechanical control system (rigid

body) submerged in a real fluid subjected to external forces can be written as:

$$\nabla_{\gamma'} \gamma' = \mathbf{G}^\#(P(\gamma(t))) + \mathbf{G}^\#(F(\gamma'(t))) + \sum_{i=1}^6 \mathbb{I}_i^{-1}(\gamma(t)) \sigma_i(t), \quad (2)$$

where $\mathbf{G}^\#(P(\gamma(t)))$ represents the potential or restoring forces and moments arising from gravity and the vehicle's buoyancy, and $\mathbf{G}^\#(F(\gamma'(t)))$ represents the dissipative drag forces and moments. The input control vector fields \mathbb{I}_i^{-1} are given by $\mathbb{I}_i^{-1} = \mathbf{G}^\# \pi_i = \mathbf{G}^{ij} X_j$, where X_1, \dots, X_6 is the standard left-invariant basis for $\text{SE}(3)$, π_1, \dots, π_6 is its dual basis and \mathbf{G}^{ij} is the i, j -entry of the kinetic energy matrix $\mathbf{G}^\#$. These input vector fields are also expressed as the i^{th} column of the matrix $\mathbb{I}^{-1} = \begin{pmatrix} M^{-1} & 0 \\ 0 & J^{-1} \end{pmatrix}$, where M and J represents the mass and inertia matrix (including added mass and the added mass moments of inertia). Finally, the $\sigma_i(t)$ are the controls. In this formulation we assume that we have six input controls that act upon each of the six degrees-of-freedom (6DOF); we assume three forces acting at the center of gravity along the body-fixed axes and three pure torques about these three body-fixed axes.

These equations, written as a first order control system on TQ , take the form

$$\begin{aligned} Y'(t) &= S(Y(t)) + \text{vlft}(\mathbf{G}^\# P(\gamma(t)))(Y(t)) + \text{vlft}(\mathbf{G}^\# F(\gamma'(t))) \\ &+ \sum_{i=1}^m \text{vlft} \mathbb{I}_i^{-1}(\gamma(t)) \sigma_i(t), \end{aligned} \quad (3)$$

which is equivalent to:

$$\dot{\mathbf{b}} = R \boldsymbol{\nu}, \quad (4)$$

$$\dot{R} = R \hat{\boldsymbol{\Omega}}, \quad (5)$$

$$M \dot{\boldsymbol{\nu}} = -\boldsymbol{\Omega} \times M \boldsymbol{\nu} + D_{\boldsymbol{\nu}}(\boldsymbol{\nu}) \boldsymbol{\nu} - g(\mathbf{b}) + \boldsymbol{\sigma}_{\nu}, \quad (6)$$

$$J \dot{\boldsymbol{\Omega}} = -\boldsymbol{\Omega} \times J \boldsymbol{\Omega} - \boldsymbol{\nu} \times M \boldsymbol{\nu} + D_{\boldsymbol{\Omega}}(\boldsymbol{\Omega}) \boldsymbol{\Omega} - g(\boldsymbol{\eta}_2) + \boldsymbol{\sigma}_{\Omega}. \quad (7)$$

Here, $(\mathbf{b}, R) \in \text{SE}(3)$, $\mathbf{b} = (b_1, b_2, b_3)^t \in \mathbb{R}^3$ denotes the position vector of the body, and $R \in \text{SO}(3)$ is a rotation matrix describing the orientation of the body. The operator $\hat{\cdot} : \mathbb{R}^3 \rightarrow \mathfrak{so}(3)$ is defined by $\hat{y}z = y \times z$. The vectors $\boldsymbol{\nu} = (v_1, v_2, v_3)^t$ and $\boldsymbol{\Omega} = (\Omega_1, \Omega_2, \Omega_3)^t$ denote the translational and angular velocities, respectively in the body-fixed frame. The drag forces and moments are accounted for in $D_{\boldsymbol{\nu}}(\boldsymbol{\nu})$ and $D_{\boldsymbol{\Omega}}(\boldsymbol{\Omega})$, respectively. Finally, $\boldsymbol{\eta}_2 = (\phi, \theta, \psi)^t$, $g(\mathbf{b})$ and $g(\boldsymbol{\eta}_2)$ represent the restoring forces and moments, respectively and $\boldsymbol{\sigma}_{\nu} = (\sigma_1, \sigma_2, \sigma_3)^t$ and $\boldsymbol{\sigma}_{\Omega} = (\sigma_4, \sigma_5, \sigma_6)^t$ account for the external control forces acting on the submerged rigid body.

Since the end goal of our control strategy design is practical implementation, we include a description of the physical parameters assumed for the test-bed vehicle upon which our calculations are based. We assume that the vehicle has three planes of symmetry and take the center of the body-fixed reference frame to be located at the center of gravity C_G . The main hull of the vehicle is assumed to be a sphere, with eight actuators positioned around the equator. These thrusters are evenly distributed around the sphere with four oriented vertically and four oriented horizontally. Additionally, we assume that the center of buoyancy (C_B) is located relatively close to C_G , with respect to the diameter of the spherical hull. Numerical values used for modeling the physical and hydrodynamic parameters of the test-bed vehicle

are presented in Table 1. These values were derived from estimations and experiments performed on the actual vehicle. Viscous drag is modeled by use of a diagonal matrix containing nonlinear terms with respect to velocity. A more detailed description of the actual

Mass	123.8 kg	$B = \rho g \mathcal{V}$	1215.8 N	C_B	(0, 0, -7) mm
Diameter	0.64 m	$W = mg$	1214.5 N	C_G	(0, 0, 0) mm
$M_f^{v_1}$	70 kg	$M_f^{v_2}$	70 kg	$M_f^{v_3}$	70 kg
I_{xx}	5.46kg m ²	I_{yy}	5.29kg m ²	I_{zz}	5.72kg m ²
$J_f^{\Omega_1}$	0kg m ²	$J_f^{\Omega_2}$	0kg m ²	$J_f^{\Omega_3}$	0kg m ²

Table 1. Main dimensions and hydrodynamic parameters.

test-bed vehicle used for implementation experiments can be found in (Chyba et al., 2009a) and (Smith, 2008). Depending upon the control strategy design method, different estimations to calculate the dissipative drag coefficients were used. The kinematic motion method estimated the drag coefficient as a function of the velocity by use of the standard formula from hydrodynamics $D = \frac{1}{2}\rho C_D v|v|$. The drag coefficient was then chosen to correspond to the average velocity of the motion. The computation of the optimal trajectories employs the STP algorithm, which encounters difficulties when presented with a non-differentiable term ($|v|$). Thus, for this trajectory design method we estimate the coefficient as a linear plus a cubic function of velocity. As previously mentioned, both estimations are based upon full-scale model tests performed on the actual test-bed vehicle used in the implementation experiments.

As previously noted, the test-bed vehicle has eight thrusters that do not act directly at C_G . The transformation between the 6DOF controls and the controls for the eight thrusters is realized via a linear matrix. Following (Chyba et al., 2009a), the relation is given by $\sigma = TCM\gamma$ where:

$$TCM = \begin{pmatrix} -e_1 & 0 & e_1 & 0 & e_1 & 0 & -e_1 & 0 \\ e_1 & 0 & e_1 & 0 & -e_1 & 0 & -e_1 & 0 \\ 0 & -1 & 0 & -1 & 0 & -1 & 0 & -1 \\ 0 & -e_3 & 0 & -e_3 & 0 & e_3 & 0 & e_3 \\ 0 & e_3 & 0 & -e_3 & 0 & -e_3 & 0 & e_3 \\ e_2 & 0 & -e_2 & 0 & e_2 & 0 & -e_2 & 0 \end{pmatrix} \tag{8}$$

$e_1 = \sqrt{2}/2, e_2 = 0.4816, e_3 = -0.2699$. In this chapter, we will refer to the control applied to the actual thrusters as the 8-dimensional (8-D) control. The thrusters are powered independently, hence the domain of control is a box in the 8-D space of the real control. We assume that all the thrusters are bounded similarly by:

$$\gamma_i \in [\gamma^{\min}, \gamma^{\max}] = [-11.7331, 9.7993] \text{ N}.$$

3. Optimization

3.1 Statement of the Problem

Control theory deals with systems that can be governed. As a consequence, it is very natural to ask for the most efficient control strategy for a given criterion. In the supplementary chapters of (Bullo & Lewis, 2004) and in (Coombs, 2000), the authors investigate mechanical

control theory and produce a version of the maximum principle for affine connection control systems. We will not discuss this approach here. Here we will state the problem, define the criterion to be minimized and introduce some terminology. This is sufficient for the purpose of this chapter. In the sequel of the chapter, a configuration at rest is a state of the system such that the velocity variables are zero.

The problem is as follows: "Given a mechanical control system and a set of initial and final configurations at rest, we would like to find a control strategy that steers the system from the initial configuration to the final configuration while minimizing a prescribed criterion." Notice that in what follows, we assume the existence of an optimal control strategy and we focus on designing such a strategy. From a mathematical point of view, a criterion is defined on a time interval $[0, T]$ by:

$$C(T, u) = \int_0^T l(t, \chi(t), \sigma(t)) dt + g(T, \chi(t)), \quad (9)$$

where l is a function that is continuously differentiable with respect to its variables and g is a continuous function. The main objective of this research is to design control strategies for an AUV that are efficient in terms of their energy consumption and time duration. The energy consumption criterion is largely dependent upon the considered mechanical system, in this chapter the criterion we use is based on our test-bed vehicle, see (Chyba et al., 2009a). The vehicle is powered solely by on-board batteries, hence its autonomous abilities are directly related to the life-span of this power supply. As seen above, the vehicle is controlled by eight external thrusters. These thrusters draw power from a bank of 20 batteries. All other on-board electronics such as the computer and sensors run on a separate bank of four batteries which supply enough power for the vehicle to operate nearly indefinitely when compared to the life-span of the thruster batteries. Thus, minimizing energy consumption for a given trajectory directly corresponds to minimizing the amount of current pulled by the thrusters. We can write the consumption criterion of the eight thrusters as:

$$C(\gamma) = \int_0^T \sum_{i=1}^8 Amps(\gamma_i(t)) dt, \quad (10)$$

where the final time T is chosen based upon how much emphasis we opt to put on the time-efficiency of the trajectory. Let T_{\min} be the minimum time to connect two terminal configurations at rest, we define c_T as:

$$T = c_T \cdot T_{\min}, \quad c_T \geq 1. \quad (11)$$

Note that the way we consider the problem, for $c_T = 1$ the solution of the minimum time and minimum consumption problems are the same. In (Chyba et al., 2009a), the authors examine the evolution of energy consumption as a function of c_T . It was found that there exists an optimal c_T that produces the best energy consumption for the vehicle, this value depends on the final configuration and on the parameters of the vehicle. The function Amps was determined experimentally on the test-bed vehicle, we found:

$$Amps(\gamma_i) = \begin{cases} -0.4433\gamma_i & = \alpha_- \gamma_i, & \text{if } \gamma_i \leq 0 \\ 0.2561\gamma_i & = \alpha_+ \gamma_i, & \text{if } \gamma_i > 0 \end{cases}, \quad (12)$$

where $Amps(\gamma_i)$ (A) is the current pulled when the thrust γ_i (N) is applied by the thruster.

3.2 Maximum Principle and Terminology

The maximum principle is one of the most fundamental tools of optimal control and provides necessary conditions for a trajectory to be optimal. We refer the reader to (Pontryagin et al., 1962) for the original text that introduced the maximum principle. See (Bonnard & Chyba, 2003), (Agrachev & Sachkov, 2004) for more modern and geometric versions and (Sussmann, 2000) for a more general version.

Let us introduce $\chi = (\eta, \nu, \Omega)$, and consider the optimal control problem of finding a path that steers our AUV from an initial configuration χ_0 to a final configuration χ_T , while minimizing an integral criterion of the form $\int_0^T l(\chi(t), \gamma(t)) dt$, where $\gamma(t)$ is the 8-D control. For instance, for the time minimization problem, we have $l(\chi, \gamma) = 1$ and for the energy consumption minimization problem, we have $l(\chi, \gamma) = \sum_{i=1}^8 \text{Amps}(\gamma_i)$ and $T = c_T T_{min}$, $c_T \geq 1$.

We will not explicitly state the maximum principle here, as it is not directly used in our numerical simulations. However, based on this principle we will introduce some terminology to describe different types of controls (see also (Sussmann, 1991)). The terminology is related to the 8-D control $\gamma = (\gamma_1, \dots, \gamma_8)^t$ introduced in Section 2, but it should be noted that this can be generalized to any other thruster configurations. A bang-bang control $\gamma_i : [0, T] \rightarrow [\gamma^{\min}, \gamma^{\max}]$ is a control that only assumes the values γ^{\min} or γ^{\max} for almost every $t \in [0, T]$. If in addition, γ_i is actually a.e. constant on $[0, T]$, then we will call it a bang control. A switching time (or simply just a switching) of γ_i is a time $t \in [0, T]$ such that γ_i is not bang on any interval of the form $(t - \delta; t + \delta) \in [0, T]$, $\delta > 0$. A control with finitely many switchings is called regular bang-bang. It is clear that a regular bang-bang control is a control composed of a finite number of concatenated bang arcs. For our purposes, we include the following additional definition. A piecewise constant (PWC) control γ_i that takes its values in the set $\Gamma_i = \{(\gamma^{\max}, \gamma^{\max}), (\gamma^{\max}, \gamma^{\min}), (\gamma^{\min}, \gamma^{\max}), (\gamma^{\min}, \gamma^{\min})\}$ is said to be a Γ_i -valued PWC control. Note that for this chapter all Γ_i are identical but it is a straightforward generalization to assume unique bounds on each individual thruster. One can then define a Γ -valued control to be bang (resp. bang-bang, regular bang-bang, Γ -valued PWC) if each of its two components is bang (resp. bang-bang, regular bang-bang, Γ_i -valued PWC). Notice that a regular bang-bang control is a Γ -valued PWC control, except that the converse is not necessary true. Another type of control, called singular, plays a major role in optimal control strategy. The definition of singular controls is related to the maximum principle and the switching functions. We do not discuss the details of a singular control here because our STP algorithm is only concerned with PWC controls, as singular controls are continuously evolving, and hence very difficult to implement on a real vehicle.

3.3 Numerical Algorithm

In (Chyba et al., 2009b) the authors conduct an analysis of the singular extremals, however it is clear that an optimal synthesis is out of reach because of the complexity of the problem. For this reason, we turn to numerical methods.

We distinguish two types of numerical methods in optimal control, namely indirect methods and direct methods. The indirect methods based on the maximum principle use shooting techniques to numerically solve a boundary value problem, see for instance (Cesari, 1983). Direct methods, on the other hand, transform the problem into a finite dimensional

optimization problem. Each method has its advantages and disadvantages. Direct methods offer less precision than indirect methods, however they are much more robust and not very sensitive to the initialization condition, contrary to indirect methods. Moreover, to apply an indirect method, we must know the structure of the optimal control in advance (such as the number of switchings, for instance). As it was shown in (Chyba et al., 2009a) the optimal control strategies for our problem are very complex and we cannot extract such information *a priori*. For these reasons we use a direct method to carry out our computations.

As mentioned, direct methods are a rewriting of the optimal control problem as a finite dimensional optimization problem. There are many ways to rewrite an optimal control problem. Here we reparameterize the time domain $[0, T]$ as $[0, 1]$, and choose a discretization $0 = t_0 < t_1 < \dots < t_N = 1$ of $[0, 1]$. Then, we write the discretized optimal control problem with unknowns $T, \chi^i = \chi(t_i), i = 1, \dots, N$ and $\gamma^i, i = 0, \dots, N - 1$. The result is a large-scale, nonlinear optimization problem whose nonlinear constraints are the discretized dynamics (for an Euler scheme) of the form $\chi^{i+1} = \chi^i + T(t_{i+1} - t_i)\dot{\chi}^i(\chi^i, \gamma^i), i = 0, \dots, N - 1$ and $\chi^N = \chi^T$. We call this the non-linear problem. Methods to solve nonlinear optimization problems are well developed. We choose to use the interior point method IpOpt (Wächter & Biegler, 2006), together with the modeling language AMPL (Fourer et al., 1993). For our direct method, we use Heun's fixed-step integration scheme.

From previous results (Chyba et al., 2009a), it is clear that the optimal control strategies are not suitable for implementation onto a test-bed vehicle (we include them in our study for the purpose of comparison). Their unsuitability is due to their complexity and the large number of actuator changes required during the implementation. The motivation to introduce the switching time parametrization (STP) algorithm was to produce efficient trajectories that are implementable on an autonomous underwater vehicle. At first, the considered cost to be minimized was time. In (Chyba et al., 2009a), the STP algorithm was used to produce efficient trajectories which optimized a combination of time and energy consumption. In the next section, we recall the important features of the STP algorithm, a detailed description can be found in the original article cited above.

3.3.1 Switching Time Parametrization Algorithm

The STP algorithm is based on the use of a direct method. The main idea is to impose the structure of the control strategy and compute trajectories having this structure that are optimal with respect to the given cost. More precisely, we fix the number of switching times along the trajectory, preferably to a small number, then we numerically determine the optimal trajectory from these candidates. Critical for the convergence of the algorithm is to introduce the values of the constant thrust arcs as parameters of the optimization problem. This new optimization problem is called $(STPP)_p$ (Switching Time Parameterization Problem) where p refers to the number of switching times. The unknowns are the time durations of the constant thrust arcs, and the values of the constant thrust arcs. Notice that our construction produces PWC control strategies, but they are not necessarily bang-bang. The new optimization problem, $(STPP)_p$,

takes the following form:

$$(STPP)_p \left\{ \begin{array}{l} \min_{z \in \mathcal{D}} t_{p+1}, \\ t_0 = 0, \\ t_{i+1} = t_i + \xi_i, \quad i = 1, \dots, p, \\ \chi^{i+1} = \chi^i + \int_{t_i}^{t_{i+1}} \dot{\chi}(t, \gamma^i) dt, \\ \chi^{p+1} = \chi^T, \\ z = (\xi_1, \dots, \xi_{p+1}, \gamma^1, \dots, \gamma^{p+1}), \\ \mathcal{D} = \mathbb{R}_+^{(p+1)} \times \mathcal{U}^{p+1}, \end{array} \right. \quad (13)$$

where $\xi_i, i = 1, \dots, p+1$ are the time arc-lengths and $\gamma^i \in \mathcal{U}, i = 1, \dots, p+1$ are the values of the constant thrust arcs.

To integrate the dynamic system of $(STPP)_p$ we use *DOP853*, a high order adaptive step integrator, (Hairer et al., 2003). The possibility of using a high-precision integrator for the *STP*-control strategies is facilitated by the fact that we drastically reduced the number of unknowns, with respect to the nonlinear problem. This results in a considerable savings in computational time with the use of our *STP* algorithm.

Finally, since the *STP* algorithm is directed towards the implementation of the control strategy onto a test-bed AUV, we add a linear junction between the constant thrust arcs to avoid instantaneous switching of the physical actuators. This linear junction has a time duration of $\delta t = 0.9 \text{ s}$ (30 refresh periods of our test-bed vehicle's CPU).

4. Simulations

As mentioned in the introduction, under-actuation plays a central part in the guidance and control of AUVs. For the following under-actuated scenario, we may assume that the AUV malfunctions for one reason or another; battery failure, an actuator quits or electronics short out. Depending on the number and arrangement of the actuators, in the event that one or more actuators stop working or is turned off, the vehicle can lose direct control in one or more degrees-of-freedom (DOF). Once we do not have direct control on all six DOF, we consider the vehicle to be under-actuated. In this scenario, the vehicle may not be able to realize any given configuration, making the motion planning problem even more difficult.

From the description of the assumed test-bed vehicle presented in section 2.1.1, we note that there are two different orientations of the thrusters. We shall call a thruster oriented such that the output force is parallel to the (body-frame) b_3 -axis a *vertical* thruster, and a thruster oriented such that the output force is perpendicular to the (body-frame) b_3 -axis a *horizontal* thruster. In this section we consider the center of gravity to be 7 mm below the center of buoyancy. This choice is motivated by experimental work that was conducted on the real vehicle, see (Chyba et al., 2008, 2009a), (Smith, 2008) and (Smith et al., 2009b). Based on these assumptions of the locations of C_G and the center of buoyancy, we may assume that a vertical thruster contributes only to heave, roll and pitch controls, while a horizontal thruster contributes only to surge, sway and yaw controls. Thus, our assumed fully-actuated submersible controls heave, roll and pitch with one set thrusters we will call V. While surge, sway, and yaw are controlled with another set of thrusters called H. Suppose for the under-actuated scenario

that we lose the ability to control either H or V. Losing control of the thruster set V would limit the motion of the vehicle to a plane. However, losing H would not affect the kinematic controllability of the vehicle; these results are proven in (Smith, 2008) and (Smith et al., 2009a).

This section is divided into three parts. First we apply the STP algorithm to the energy consumption cost and design implementable trajectories for the presented under-actuated scenario. Secondly, from previous work, we recall control strategies for the identical under-actuated scenario designed by the use of kinematic motions. We conclude with a comparison of both control strategies.

4.1 Mission Scenario 1

Based on the controllability results mentioned previously, we assume that we only have direct control of the vertically-oriented thrusters. We first demonstrate that the vehicle can realize motion in a direction that is not directly controllable. Suppose that we would like our vehicle to realize a pure surge displacement. From our previous assumptions, we have no control of the horizontally-oriented thrusters, thus we do not have the use of the input control vector field \mathbb{I}_1^{-1} . We only have direct control upon roll, pitch and heave (i.e., $\{\mathbb{I}_3^{-1}, \mathbb{I}_4^{-1}, \mathbb{I}_5^{-1}\}$). Is it possible to reach $\eta_{final} = (a, 0, 0, 0, 0, 0)$, for $a \in \mathbb{R}$, in this proposed under-actuated condition? From Proposition 4.1 of (Smith, 2008), we can compute that the vehicle is kinematically controllable, and hence, the answer to the question is yes; any configuration is reachable from any other via kinematic motions. This fact is also proven in (Smith et al., 2009a), however, a simple calculation shows that $\text{Lie}^\infty(\mathbb{I}_3^{-1}, \mathbb{I}_4^{-1}, \mathbb{I}_5^{-1}) = TQ$. Let us choose $a = 1.25$ m. Since we have direct control of the pure heave motion, and we assume a positively buoyant vehicle, it is clear that reaching the configuration $\eta_{final} = (1.25, 0, b, 0, 0, 0)$, for $b \in \mathbb{R}^+$, will prove that the vehicle can realize the prescribed surge displacement. We choose $\eta_{final} = (1.25, 0, 2.165, 0, 0, 0)$ as the goal configuration for this mission. Below we present two methods to accomplish this displacement.

4.1.1 STP motions

In this section, we present a complete study for trajectories ending at the final configuration η_{final} chosen above. First, we compute the minimum time and minimum energy consumption trajectories, without imposing any implementation restriction. Then, we apply the STP algorithm to the same final configuration and compare our results to the optimal ones.

Assuming failure of all the horizontal thrusters, the minimum time control strategy to steer the AUV from the origin to η_{final} can be seen in Figure 1. Notice that we represent the control in the 6DOF rather than in 8 dimensions to emphasize the fact that our approach is valid for other thrusters configurations. The minimum time is approximately $t_{min}^{1,vert} \approx 11.249011$ s with a corresponding energy consumption of $C_{t_{min}^{1,vert}} \approx 199.476331$ A.s. As it can be seen in Figure 1, the computed trajectory consists of a large pitch angle followed by significant thrust in the heave direction of the body-fixed frame. We remark that the minimum time for the same initial and final configurations, but in the fully actuated case, is $t_{min}^1 \approx 7.535102$ s with a corresponding energy consumption of $C_{t_{min}^1} \approx 235.141099$ A.s. Thus, losing the use of the horizontal actuators, the time optimal trajectory is 49% longer but we use 15% less energy.

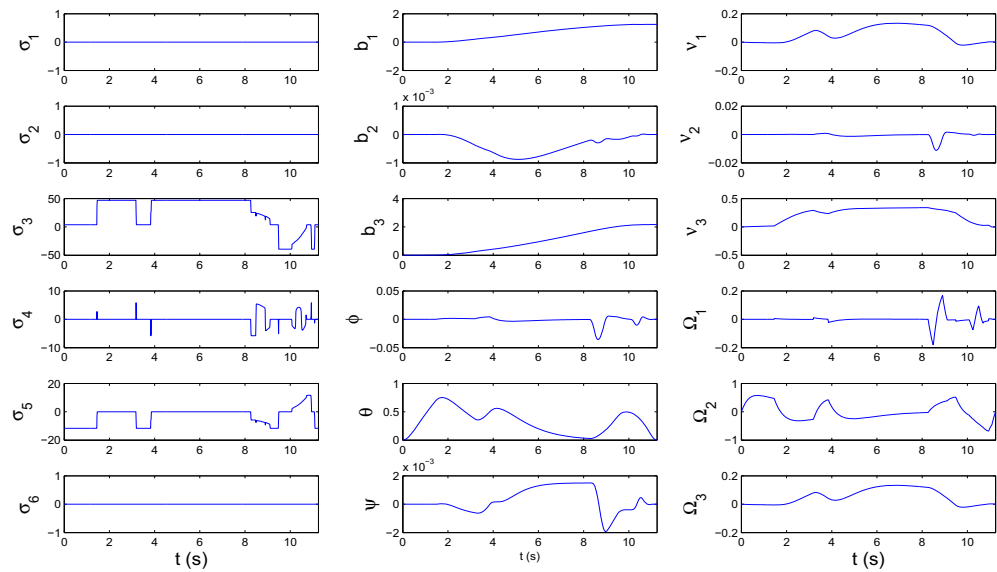


Fig. 1. Minimum time solution for η_{final} and failure of the horizontal thrusters.

Figure 2 shows the solution to the minimum energy consumption problem in the under-actuated situation with a final time of $t_f = 16.6\text{ s}$, which correspond to $c_T = t_f/t_{\min}^{1,vert} \approx 1.47$. The minimum energy consumption control strategy consumes $C_{\min}^{1,vert} \approx 93.389150\text{ A.s}$, which

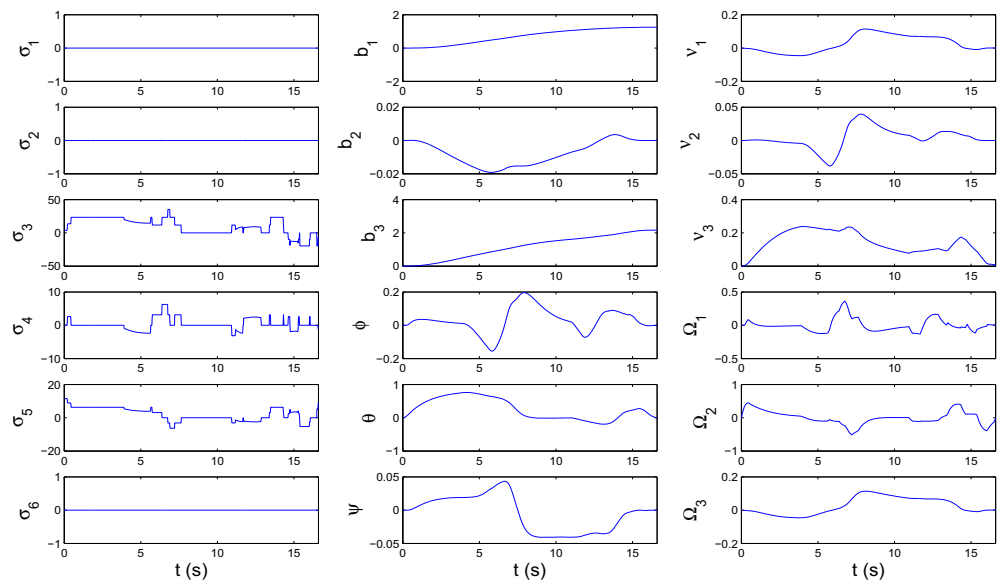


Fig. 2. Minimum consumption solution for η_{final} , $t_f = 16.6\text{ s}$ and failure of horizontal thrusters.

represents a gain of slightly more than 53% when compared to the under-actuated time minimum trajectory. A larger reduction in energy consumption could be realized if we were to allow more time. Our choice of the final time here is dictated by our desire to compare

our results to those calculated by use of kinematic motions. In the fully actuated case, the minimum energy consumption is given by $C_{\min}^1 \approx 69.746188$ A.s. This represents about 3.37 times less energy than is consumed during the fully-actuated time minimum trajectory. The fact that the gain is more significant in the fully-actuated case is that this situation corresponds to a c_T coefficient of $t_f/t_{\min}^1 \approx 2.2$, which is closer to the optimal c_T corresponding to this mission.

Application of our STP algorithm to the under-actuated time minimum problem, we obtain the results shown in Table 2. We remark that it is quite surprising to see the existence

#switch	t_{\min} (s)	Cons. (A.s)	switching times (s)
2	16.002832	148.895085	(11.4449, 13.3028)
3	15.634220	148.640740	(8.5415, 11.0682, 12.9342)
4	≈ 15.620850	147.826597	(6.8255, 8.6255, 11.1208, 12.9208)
5	≈ 15.606090	157.978504	(4.3083, 6.8127, 8.6477, 11.1053, 12.9057)

Table 2. STP minimum time for horizontal thruster failure.

of an admissible STP control strategy with only 2 switching times. To reach a final time close to the optimal time, we need to increase the number of switching times. The STP trajectory with two switching times is about 40% slower than the time minimal trajectory. Notice that the trajectories with an approximation sign in front of the minimum time are strategies for which the STP method did not converge to a solution satisfying the first order necessary condition, but nevertheless, provided and admissible strategy.

The STP algorithm applied to the under-actuated scenario for the minimization of energy consumption with a final time of 16.6s is given in Table 3. We notice a gain of 7% in the

#switch	Consumption (A.s)	switching times (s.)
2	150.253134	(11.7619, 13.9000)
3	137.254314	(7.3433, 12.1000, 13.9000)
4	126.330384	(7.5304, 10.3000, 12.1000, 13.9000)

Table 3. STP minimum consumption for horizontal thruster failure and $t_f = 16.6$ s.

case of three switching times and a gain of about 15% in the case of 4 switching times. The controls and the trajectory are respresented on Figure 6 below for the two switching times strategy.

4.1.2 Kinematic motions

This section recalls the results from (Smith, 2008) and (Smith et al., 2009a) on control strategies obtained through the use of kinematic motions. We refer the reader to these references for more theoretical details on the control strategies depicted below and to (Bullo & Lewis, 2004) for a general treatise on kinematic reductions for mechanical control systems.

One way to reach the desired configuration is to pitch the vehicle an angle α and hold this pitch angle while applying a body-pure heave (i.e., apply a control along the z-axis of

the body-fixed reference frame) until the vehicle realizes the 1.25 m surge displacement. The value of α depends upon the final configuration. For this experiment, we must take $\alpha = 30^\circ$, which corresponds to $b = 2.165$ m. A general depiction of this motion is presented in Figure 3.

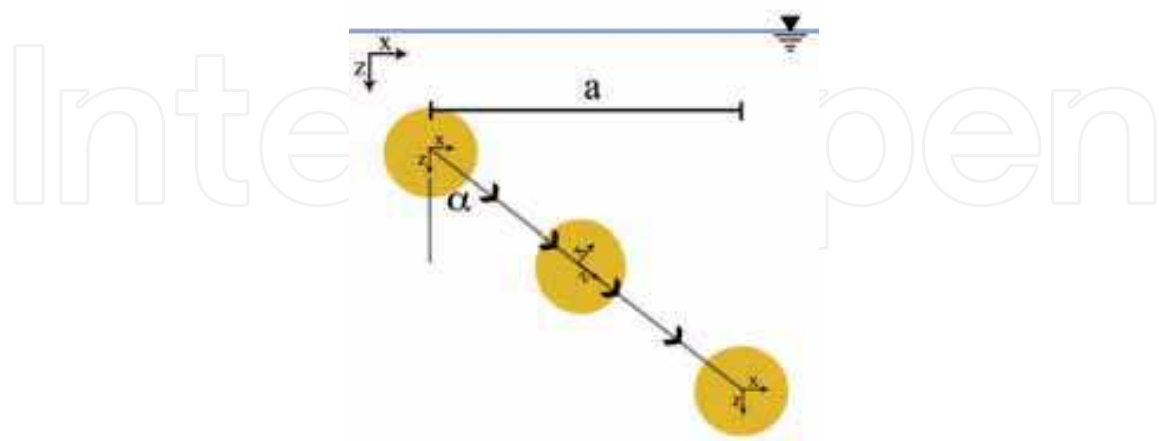


Fig. 3. A generalization of the intended trajectory designed with kinematic motions.

With $\eta_{final} = (1.25, 0, 2.165, 0, 0, 0)$, we present two separate control strategy designs for this mission. Given that the set of input control vector fields is $\mathcal{I}_3^{-1} = \{\mathbb{I}_3^{-1}, \mathbb{I}_4^{-1}, \mathbb{I}_5^{-1}\}$, the decoupling vector fields for this system are the constant multiples and linear combinations of the set $\mathcal{D} = \{X_3 = (0, 0, 1, 0, 0, 0), X_4 = (0, 0, 0, 1, 0, 0), X_5 = (0, 0, 0, 0, 1, 0)\}$, see (Smith et al., 2009a).

The basic idea of this motion is to point the bottom of the AUV at η_{final} by following the integral curves of X_4 (pitch motion), then follow the integral curves of X_3 (body-pure heave motion) to realize the displacement. At the end of the body-pure heave motion, the vehicle will be in the configuration $(1.25, 0, 2.165, 0, 30^\circ, 0)$. We can undo the pitch motion by following the integral curves of $-X_4$, however, in practice, the righting moments take care of this angular displacement without having to apply any control forces; thus saving energy. It is important to notice that for the mathematical model using the righting moments to bring back the vehicle into a zero pitch angle takes a very large time because the coordinate θ actually oscillates around the zero. So it is a very efficient option for the experimental aspect of the project as the vehicle is asked to reach the final configuration within a prescribed tolerance and not exactly.

If we want to realize a surge displacement greater than 1.25 m, we may concatenate the following designed trajectory with one using the negative of the prescribed roll angle and body-pure heave control to create a V-shaped motion, as depicted in Figure 4. This would realize a 2.5 m displacement. Concatenating more V-shaped motions will allow for greater surge displacements.

On the other hand, we could successively implement the trajectory given here followed by a pure heave motion of 2.165 m. This would create a sawtooth-type trajectory as shown in Figure 5.

The distance of 1.25 m is arbitrarily chosen and depends upon the pitch angle prescribed as well as the length of the body-pure heave motion. Altering each of these, we can also create

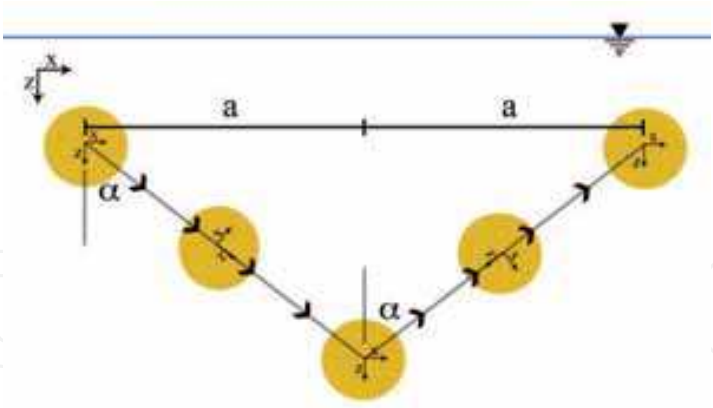


Fig. 4. Concatenation of the presented kinematic motion trajectory to create a V-shaped motion.

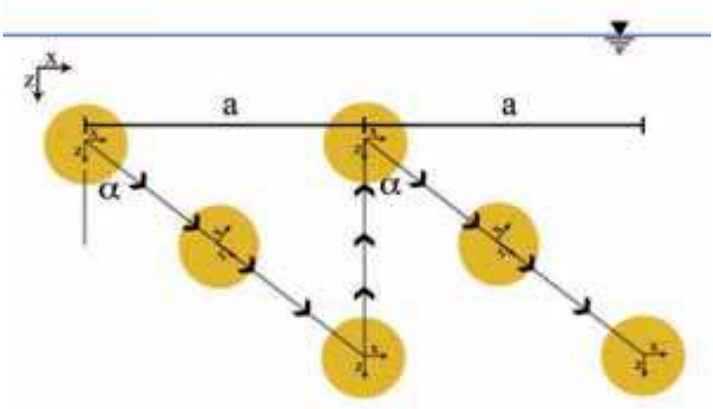


Fig. 5. Successive concatenation of the presented trajectory with pure heave motions to create a sawtooth-shaped motion.

different surge displacements.

The six-dimensional under-actuated control strategy for the kinematic motion is given at Table 4 (the times represent the junction times of the PWC strategy).

Time (s)	Applied Thrust (6-dim.) (N)
0	(0,0,0,0,0,0)
0.9	(0,0,1.126,0,4.2553,0)
5.9	(0,0,1.126,0,4.2553,0)
6.8	(0,0,31.166,0,4.2553,0)
12.373	(0,0,31.166,0,4.2553,0)
13.273	(0,0,-23.431,0,4.2553,0)
15.7	(0,0,-23.431,0,4.2553,0)
16.6	(0,0,0,0,0,0)

Table 4. Discretized control structure using kinematic motions.

This control strategy has two swithcing times and the energy consumed for the above trajectory is 138.458 A.s. This control strategy has been calculated in several steps. First differential geometric techniques are used to generate a continuous control as a function of time. But as discussed earlier, input for the test-bed vehicle requires a PWC control structure over discretized time intervals with in addition linear junctions to link the constant arcs. Hence the second step of the process is to adapt the continuous control into a PWC control. This is done by ensuring that the work required to perform the desired motion is equivalent for both the continuous and PWC control, see (Smith, 2008) for more details. The last step is to simply connect the constant arcs via linear junctions of 0.9 seconds.

4.1.3 Comparison

The control strategy based on decoupling vector fields was calculated by applying inverse kinematics to the concatenation of kinematic motions available to the under-actuated vehicle. During the trajectory design phase of this process, one is allowed to arbitrarily parameterize the time necessary to traverse the chosen path. In the presented example, the parameterization was chosen so that the test-bed vehicle could perform the given motion at a normal operational velocity. Such a choice of parameterization did not take into account any time or energy consumption optimization. However, the ability to reparameterize the duration of the kinematic motion does give rise to the question of whether or not this type of trajectory design can be made time or energy optimal.

Our intent here is to compare the STP control strategies to the one derived from the kinematic motion. But the comparison is not completely straightforward. Indeed, we have to keep in mind that the discretized control given in Table 4 is an adaptation of the continuous control strategies calculated as a concatenation of integral curves of kinematic reduction of rank one. The procedure to compute the PWC control and the addition of the linear junction were introduced for the purpose of implementation on our test-bed vehicle. A consequence is that we obtained a control easily implementable but that as the disadvantage to not exactly reached the desired configuration. It is also very important to remember that in the design of the kinematic discretized control we use the fact that in practice the vehicle will bring back the pitch angle to zero on its own which is once again unrealistic from the mathematical model point of view. On the other extreme the STP trajectories are designed to reach exactly the final configuration and hence are more constrained. No consideration on the experimental aspect is taken into account while computing that controls. Notice that comparison of the STP trajectories with the continuous control obtained via kinematic reduction would not make sense because for the continuous motion the bounds of the control are not taken into account. It is only during the second step of the procedure when computing the PWC adaptation that we design a control satisfying the constraint of the domain of control.

In Figure 6 we represent the following three control strategies and their corresponding trajectories. The solid line represents the STP strategy, the dashed line is the discretized kinematic motion strategy and in dotted line is the minimum consumption strategy. All three strategies are defined on the same time interval $[0, 16.6]$. A first remark concern the type of control involved in these three strategies. From the maximum principle, we know that the minimum consumption control strategy is a concatenation of bang and singular arcs for the 8 dimensional control (here we represent the 6DOF control). This strategy a large number of switching times and hence is not implementable on a test-bed vehicle. The STP and

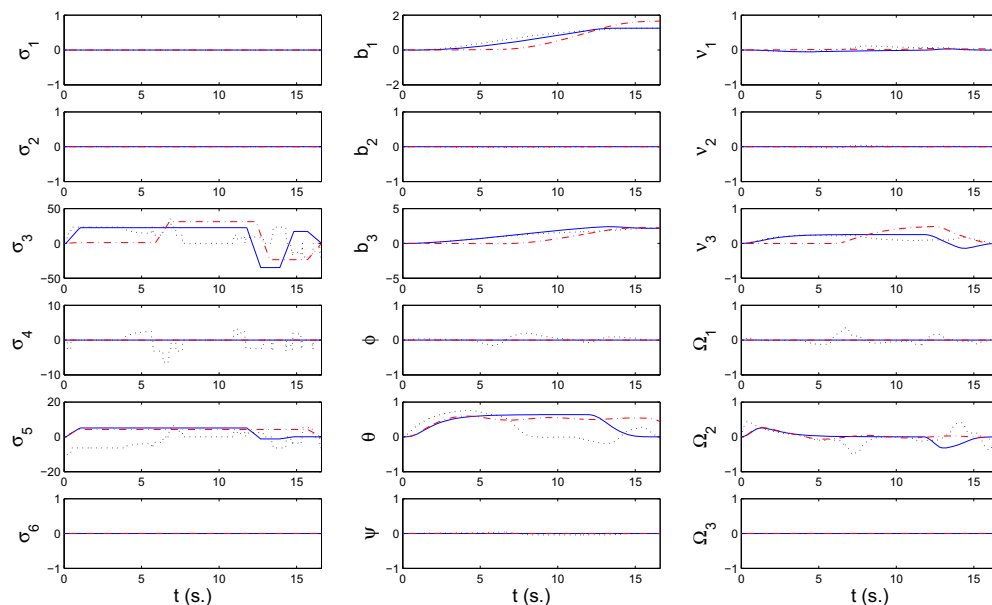


Fig. 6. Minimum consumption (dotted), STPP with 2 switching times (plain) and discretized kinematic motion (dashed).

discretized kinematic control strategies are obtained from PWC controls with the addition of linear junction to avoid instantaneous actuator changes. Notice that the switching times are differently distributed along the trajectory. However, if we look at the trajectories themselves they are quite comparable. The major difference can be seen in the θ variable where the discretized kinematic motion does not end-up at zero. This is due to the fact that, in practice, the righting moment will compensate for this error. The energy consumption for these three strategies is respectively 93.39, 153.47 and 138.46. It is surprising that the STP control strategy consumes more energy than the discretized kinematic motion. This is explained by our first observation that they do not reach the exact same final configuration and mostly because in the discretized kinematic motion, the righting moment is used during the experimentation to bring θ back to zero. To fully compare these strategies, future work will consist in experimental testing to extract the energy consumption the test-bed vehicle used during the experiment (and not the energy consumption corresponding to the simulation on the mathematical model) for both strategies and compare the results.

4.2 Mission Scenario 2

For the second mission we would like to realize a pure surge motion. Here we consider a 2.5 m pure surge while maintaining a constant depth, hence we have $\eta_f = (2.5, 0, 0, 0, 0, 0)$.

4.2.1 STP motions

In the fully actuated case the minimum time is approximately $t_{\min}^2 \approx 8.564220$ s, while the corresponding consumption is $C_{t_{\min}^2} \approx 269.422890$ A.s. The trajectory consists in a very large pitch angle in order to maximize the thrust available to travel along the b_1 direction. In the case of the failure of the horizontal thrusters the minimum time is approximately $t_{\min}^2 \approx 16.794176$ s, while the corresponding consumption is $C_{t_{\min}^2, \text{vert}} \approx 255.853619$ A.s.

Notice that the duration is almost double without the vertical thrusters but that the energy consumption is almost identical.

The solution of the minimum consumption problem with failure of the horizontal thrusters is given on Figure 7 for $t_f = 17.7\text{ s}$. The minimum consumption is $C_{\min}^{2,vert} \approx 157.115555\text{ A.s}$

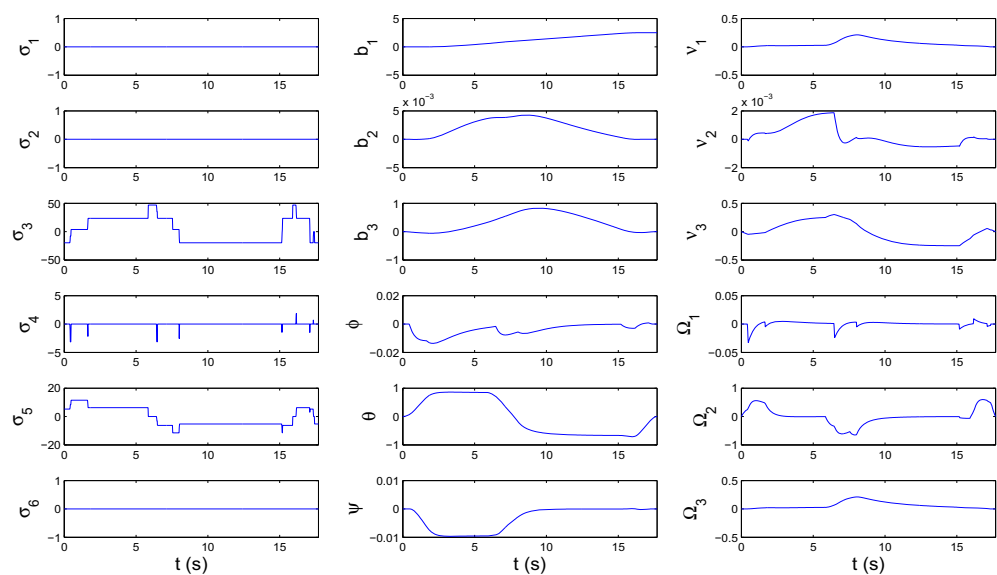


Fig. 7. Minimum consumption solution in the under-actuated case.

which represents a gain of 38.6%. This apparent small gain in consumption becomes much more significant when coupled with the fact that the prescribed final time is extremely close to the minimum time; we have $c_t = 1.05$. Once again the final time was chosen with respect to the kinematic motion that will be described below. In the fully actuated case (presented in Figure 8), we have $c_T = 2.07$ and the minimum consumption is $C_{\min}^2 \approx 54.769702\text{ A.s}$, which represents a gain of almost 80%.

Table 5 gives the values obtained when applying the STP algorithm for the energy consumption minimum problem to the fully actuated case with a final time of 17.7s. The STP control

#switch	Consumption (A.s)	switching times (s)
1	79.544612	13.6427
2	≈ 68.489915	(8.8584, 14.9966)
3		No better than 2 switchings
4	≈ 61.851409	(3.2792, 8.2950, 11.4516, 14.9999)

Table 5. STPP minimum consumption .

strategy with one switching in the fully actuated case represents about 70% less consumption of energy with respect to the minimum time solution and about 45% more consumption of

energy with respect to the minimum consumption solution. The STP control strategy for one switching time as well as its corresponding trajectory are represented in Figure 8.

4.2.2 Kinematic motions

The six-dimensional discretized control strategy is given in Table 6. This motion was param-

Time (s)	Applied Thrust (6-dim.) (N)
0	(0,0,0,0,0,0)
0.9	(12.128,0,1.3,0,0,0)
12.49	(12.128,0,1.3,0,0,0)
13.39	(-7.35,0,1.3,0,0,0)
16.8	(-7.35,0,1.3,0,0,0)
17.7	(0,0,0,0,0,0)

Table 6. Discretized control strategy.

eterized to last for 17.7 s, and consumed a total of 99.167 A.s of energy. Note that for this control strategy, we use the horizontally-oriented thrusters to realize the surge motion, while utilizing the vertically-oriented thrusters to counteract the positive buoyancy of the vehicle to maintain a constant depth. Thus, we must be fully-actuated to implement this control strategy. We can compare this to a 33.2 s duration for the V-shaped concatenated motion, which would consume 276.916 A.s of energy. This is near twice the time and three times the energy consumption. If we assume that we use the vehicle’s positive buoyancy to achieve the pure heave motion in the sawtooth trajectory, thus expending no energy along that portion, we have an overall time greater than 33.2 s and an energy consumption of 276.916 A.s.

4.2.3 Comparison

We begin with the initial remark that in the under-actuated scenario, one may initially think that the use of less actuators results in expending less energy. Here, we show that this is not the case. For the under-actuated kinematic motion presented, the energy used to maintain the list angle α requires the available actuators to expend excessive of energy for the duration of the mission. There are many ways to design a trajectory by the use of kinematic motions, and here we only present one. It would be interesting to explore the energy consumption minimization problem for kinematic motions that have the same final configuration and duration. In conclusion, in the event of an actuator failure or other malfunction, the under-actuated kinematic motion would definitely get the vehicle back home, however this motion would not be the best choice to conserve battery life while on deployment.

In Figure 8 the following three control strategies can be seen: the minimum consumption (dotted), the STP with one switching time (solid) and the discretized kinematic motion (dashed). All these are calculated for a fully actuated vehicle. We can see that the STP and kinematic motion are very similar in terms of control strategy and trajectory. However, the STP trajectory uses almost 20% less energy than the kinematic motion. The control strategy that minimizes the energy consumption differs much more dramatically from the other ones, in particular it shows a very large number of switching times and concatenations between bang and singular arcs. The trajectory differs only for the roll angle and the angular velocity Ω_3 . The main advantage regarding the STP trajectory in this

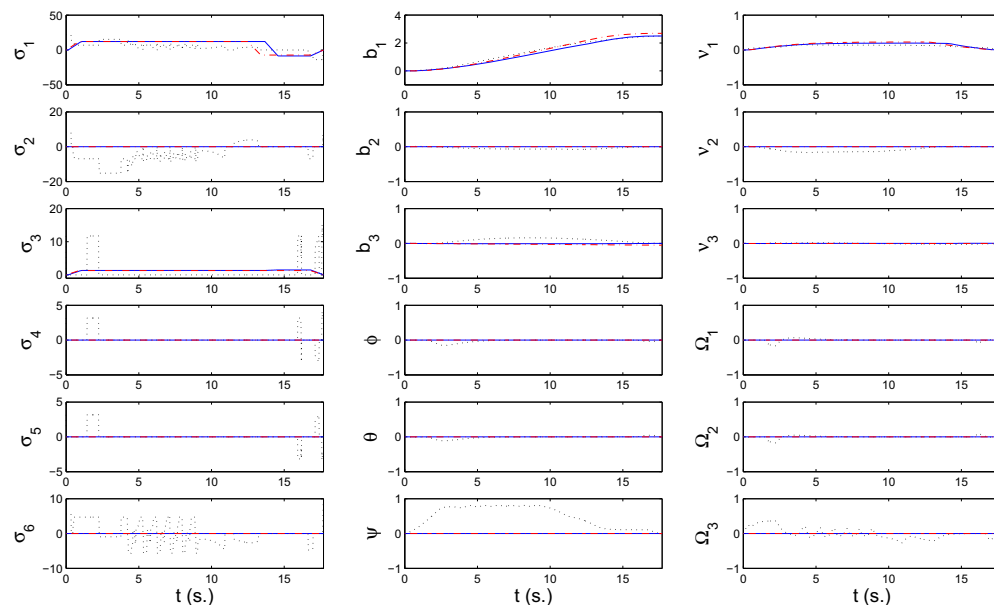


Fig. 8. Minimum consumption (dotted), STPP with 1 switching time (solid) and discretized kinematic motion (dashed) for Mission 2.

mission scenario concerns the under-actuated case. The discretized PWC kinematic motion, as presented here, would produce an extremely inefficient control strategy in terms of energy consumption while the STP algorithm would provide a much better solution (not presented in this paper).

5. Acknowledgments

The authors would like to thank the National Science Foundation for their support. The research presented in this paper is supported by NSF Grants DMS-030641 and DMS-0608583.

6. References

- Agrachev A.A.; Sachkov Y.L. (2004) Control Theory from the Geometric Viewpoint. *Springer-Verlag, Series: Encyclopaedia of Mathematical Sciences*, Vol. 87, Control Theory and Optimization, 412 pages.
- Bonnard B.; Chyba M. (2003) Singular Trajectories and their Role in Control Theory. *Springer-Verlag, Series: Mathematics and Applications*, Vol 40, 357 pages.
- Bullo F.; Lewis, A. D. (2004), Geometric Control of Mechanical Systems, *Springer-Verlag, New York-Heidelberg-Berlin*, Number 49 in Texts in Applied Mathematics, 726 pages.
- Cesari L. (1983) Optimization Theory and Applications. Problems with Ordinary Differential Equations. *Springer-Verlag*, New York, 542 pages.
- Chyba M.; Haberkorn T.; Smith R.N.; Choi S.K. (2008) Design and implementation of time efficient trajectories for an underwater vehicle. *Ocean Engineering*, 35/1, pp. 63-76.

- Chyba M.; Haberkorn T.; Singh S.B.; Smith R.N.; Choi S.K. (2009a) Increasing Underwater Vehicle Autonomy by Reducing Energy Consumption. *Ocean Engineering, Special Issue on Autonomous Underwater Vehicles*, Vol 36/1, pp. 62-73.
- Chyba M.; Haberkorn T.; Smith R.N.; Wilkens G.R (2009b) A Geometric Analysis of Trajectory Design for Underwater Vehicles. *Discrete and Continuous Dynamical Systems-B*, Volume: 11, Number: 2.
- Coombs T.A. (2000) Time-optimal control of two simple mechanical systems with three degrees of freedom and two inputs. *MSc Thesis*, Queen's University.
- Fourer R.; Gay D.M.; Kernighan B.W. (1993) AMPL: A Modeling Language for Mathematical Programming. *Duxbury Press*, Brooks-Cole Publishing Company.
- Fossen T.I. (1994) Guidance and Control of Ocean Vehicles, *John Wiley & Sons*.
- Ledzewicz U; Schättler H. (2009) On The Optimality Of Singular Controls For A Class of Mathematical Models For Tumor Anti-Angiogenesis. *Discrete and Continuous Dynamical Systems Series B*, Vol 11, Number 3, pp. 691-715.
- Lewis A.; Murray R. (1997) Configuration Controllability of Simple Mechanical Control Systems. *SIAM Journal on Control and Optimization archive*, Vol 35/3, pp. 766 - 790.
- Lewis A. (2007) Is it Worth Learning Differential Geometric Methods for Modelling and Control of Mechanical Systems? *Robotica*, 25(6), pp. 765-777.
- Pontryagin L.S.; Boltyanski B.; Gamkrelidze R.; Michtchenko E. (1962) The Mathematical Theory of Optimal Processes. *Interscience*. New York.
- Smith R.N. (2008) Geometric Control Theory and its Application to Underwater Vehicles. *PhD Dissertation*, University of Hawai'i at Manoa.
- Smith R.N.; Chyba M.; Wilkens G.R.; Catone C. (2009a) A geometrical approach to the motion planning problem for a submerged rigid body. *International Journal of Control*. Volume 82, Issue 9, pp. 1641 - 1656.
- Sussmann H.J.; Tang G. (1991) Shortest paths for the Reeds-Shepp car: a worked out example of the use of geometric techniques in nonlinear optimal control. *Rutgers Center for Systems and Control (Sycon) Report 91-10*.
- Sussmann H.J. (2000) New Theories of set-valued Differentials and new versions of the Maximum Principle of Optimal Control Theory. *Published in the book Nonlinear Control in the Year 2000*, A. Isidori, F. Lamnabhi-Lagarigue and W. Respondek Eds.; Springer-Verlag, pp. 487-526.
- Wächter A.; Biegler L.T. (2006) On the Implementation of an Interior-Point Filter-Line Search Algorithm for Large-Scale Nonlinear Programming. *Research Report RC 23149*, IBM T.J. Watson Research Center, Yorktown, New York.



Modelling Simulation and Optimization

Edited by Gregorio Romero Rey and Luisa Martinez Muneta

ISBN 978-953-307-048-3

Hard cover, 708 pages

Publisher InTech

Published online 01, February, 2010

Published in print edition February, 2010

Computer-Aided Design and system analysis aim to find mathematical models that allow emulating the behaviour of components and facilities. The high competitiveness in industry, the little time available for product development and the high cost in terms of time and money of producing the initial prototypes means that the computer-aided design and analysis of products are taking on major importance. On the other hand, in most areas of engineering the components of a system are interconnected and belong to different domains of physics (mechanics, electrics, hydraulics, thermal...). When developing a complete multidisciplinary system, it needs to integrate a design procedure to ensure that it will be successfully achieved. Engineering systems require an analysis of their dynamic behaviour (evolution over time or path of their different variables). The purpose of modelling and simulating dynamic systems is to generate a set of algebraic and differential equations or a mathematical model. In order to perform rapid product optimisation iterations, the models must be formulated and evaluated in the most efficient way. Automated environments contribute to this. One of the pioneers of simulation technology in medicine defines simulation as a technique, not a technology, that replaces real experiences with guided experiences reproducing important aspects of the real world in a fully interactive fashion [iii]. In the following chapters the reader will be introduced to the world of simulation in topics of current interest such as medicine, military purposes and their use in industry for diverse applications that range from the use of networks to combining thermal, chemical or electrical aspects, among others. We hope that after reading the different sections of this book we will have succeeded in bringing across what the scientific community is doing in the field of simulation and that it will be to your interest and liking. Lastly, we would like to thank all the authors for their excellent contributions in the different areas of simulation.

How to reference

In order to correctly reference this scholarly work, feel free to copy and paste the following:

M. Chyba, T. Haberkorn and R.N. Smith (2010). Optimization Problems for Controlled Mechanical Systems: Bridging the Gap between Theory and Application, *Modelling Simulation and Optimization*, Gregorio Romero Rey and Luisa Martinez Muneta (Ed.), ISBN: 978-953-307-048-3, InTech, Available from:
<http://www.intechopen.com/books/modelling-simulation-and-optimization/optimization-problems-for-controlled-mechanical-systems-bridging-the-gap-between-theory-and-applicat>

INTECH
open science | open minds

InTech Europe

University Campus STeP Ri

InTech China

Unit 405, Office Block, Hotel Equatorial Shanghai

www.intechopen.com

Slavka Krautzeka 83/A
51000 Rijeka, Croatia
Phone: +385 (51) 770 447
Fax: +385 (51) 686 166
www.intechopen.com

No.65, Yan An Road (West), Shanghai, 200040, China
中国上海市延安西路65号上海国际贵都大饭店办公楼405单元
Phone: +86-21-62489820
Fax: +86-21-62489821

IntechOpen

IntechOpen

© 2010 The Author(s). Licensee IntechOpen. This chapter is distributed under the terms of the [Creative Commons Attribution-NonCommercial-ShareAlike-3.0 License](https://creativecommons.org/licenses/by-nc-sa/3.0/), which permits use, distribution and reproduction for non-commercial purposes, provided the original is properly cited and derivative works building on this content are distributed under the same license.

IntechOpen

IntechOpen